Biomaterials Science

Accepted Manuscript

This article can be cited before page numbers have been issued, to do this please use: T. Katayama, A. Matsumoto, Y. Takazawa, M. Hashino, M. Kaito, Y. Chigi and D. Okamura, *Biomater. Sci.*, 2026, DOI: 10.1039/D6BM00313C.

ROYAL SOCIETY OF CHEMISTRY

rsc.li/biomaterials-science

View Article Online
DOI: 10.1039/D6BM00313C

Title: Vitronectin establishes a differentiation-restrictive extracellular microenvironment that sustains myoblast proliferation across species.

Tomoka Katayama[1], Anmi Matsumoto[1], Yoka Takazawa[1], Momoka Hashino[1], Kaito Minoru[1], Yuta Chigi[2], Daiji Okamura[1*]

[1]Department of Advanced Bioscience, Faculty of Agriculture, Kindai University, Nara 631-8505, Japan

[2]Independent researcher, Tokyo, Japan

[*]Corresponding author

E-mail: dokamura@nara.kindai.ac.jp

Telephone: +81-742-43-5384

View Article Online
DOI: 10.1039/D6BM00313C

Abstract:

The extracellular matrix (ECM) critically regulates cell fate decisions, yet matrix components that actively impose differentiation-restrictive states remain insufficiently defined. Here, we identify vitronectin (VN), a major serum-derived ECM glycoprotein, as a differentiation-restrictive matrix component that stabilizes a proliferation-competent microenvironment for myoblast expansion. Substrate-associated VN suppresses myogenic differentiation while sustaining proliferative activity in an integrin αvβ3‑dependent manner. These effects are conserved across multiple myoblast systems, including mouse C2C12, rat L6, human LHCN-M2, and primary embryonic chicken myogenic cells, demonstrating cross-species robustness. Furthermore, we show that serum-dependent differences in VN abundance directly influence myogenic differentiation, indicating that ECM composition is a critical determinant of differentiation outcomes. Under defined serum-free conditions, VN in combination with leukemia inhibitory factor (LIF) supports sustained proliferation while preserving differentiation competence, establishing a controllable expansion platform. Together, these findings redefine vitronectin as an ECM component that enforces a differentiation-restrictive microenvironment and provide a framework for matrix-driven control of progenitor cell fate.

View Article Online
DOI: 10.1039/D6BM00313C

Keywords:

Vitronectin, Extracellular microenvironment, Integrin αvβ3, Myoblast proliferation, Myogenic differentiation, Differentiation-restrictive matrix, Serum-free expansion, Cross-species conservation

Introduction:

The extracellular matrix (ECM) is now widely recognized as an active regulator of cell behavior rather than a passive structural scaffold. In addition to providing mechanical support, ECM components function as dynamic signaling interfaces that integrate adhesive interactions with intracellular pathways governing cell survival, proliferation, and lineage progression [1–4]. In engineered culture systems, matrix composition critically influences cell state transitions, underscoring the importance of cell–matrix interactions in controlling phenotypic outcomes [2,4]. Identifying ECM elements that stabilize specific cellular states therefore represents a central objective in biomaterials research and microenvironmental engineering.

Skeletal muscle differentiation provides a well-defined model for examining matrix-dependent regulation of cell fate. Myoblasts must maintain a tightly regulated balance between proliferative expansion and terminal differentiation, a transition governed by coordinated extracellular cues [5,6]. In

View Article Online
DOI: 10.1039/D6BM00313C

vitro, murine C2C12 myoblasts represent a classical system for studying myogenic differentiation, where robust myotube formation is typically induced by switching from growth medium supplemented with fetal bovine serum (FBS) to low-serum differentiation medium containing horse serum (HS) [7,8]. This widely adopted paradigm has historically been attributed primarily to the withdrawal of soluble mitogenic factors, particularly fibroblast growth factor (FGF) signaling [6,9]. However, serum replacement simultaneously alters the extracellular matrix environment, suggesting that matrix-associated components may also contribute to the regulation of myogenic commitment [10,11].

Numerous ECM substrates, including fibronectin, collagens, and laminins, have been shown to support myoblast adhesion, fusion, and differentiation, and are therefore regarded as differentiation-permissive environments [12–16]. In contrast, ECM components that actively impose differentiation-restrictive states remain poorly characterized. This emphasis on differentiation-permissive matrices, and the limited characterization of differentiation-restrictive ECM components, hinders a comprehensive understanding of how extracellular microenvironments regulate the transition from proliferation to terminal differentiation. From a biomaterials perspective, differentiation-restraining matrices are of particular interest because they may enable controlled expansion of progenitor populations prior to lineage commitment.

View Article Online
DOI: 10.1039/D6BM00313C

Vitronectin (VN) is a major serum-derived glycoprotein with well-established roles in cell adhesion and integrin-mediated signaling [17,18]. As a ligand for integrins such as αvβ3, VN participates in diverse cellular processes—including migration, survival, and proliferation—across multiple cell types [3,19]. Despite its abundance in serum and its well-recognized roles in ECM-mediated signaling, the potential function of VN in myogenic regulation has received little attention. Given that serum composition differs substantially between FBS-based growth conditions and HS-based differentiation conditions, we hypothesized that vitronectin may influence myoblast state transitions through matrix-dependent mechanisms.

Here, we investigate the functional role of vitronectin as an extracellular regulator of myoblast behavior. We demonstrate that substrate-associated VN suppresses myogenic differentiation while sustaining proliferative activity in an integrin αvβ3–dependent manner. Furthermore, we show that serum-dependent VN abundance is a key determinant of differentiation outcomes and that VN exerts conserved effects across multiple myoblast systems, including rodent, human, and primary cells. In addition, we establish a defined serum-free culture system in which VN, in combination with leukemia inhibitory factor (LIF), supports sustained myoblast expansion while preserving differentiation competence. Together, these findings identify vitronectin as a differentiation-restrictive ECM

View Article Online
DOI: 10.1039/D6BM00313C

component and highlight serum-derived matrix factors as critical regulators of myoblast fate within engineered extracellular microenvironments.

Materials and Methods:

Cell Culture

C2C12 myoblasts (an immortalized mouse myoblast cell line) [7,8] were maintained in growth medium (GM) consisting of Dulbecco's Modified Eagle Medium (DMEM) (FUJIFILM Wako, 043-30085) supplemented with 10% fetal bovine serum (FBS; Gibco, 10270-106) and 1× penicillin-streptomycin mixed solution (P/S; FUJIFILM Wako, 168-23191). Cells were passaged every 3–4 days using TrypLE (Gibco, 12604-013) at a split ratio of 1:5. For differentiation experiments, 3.0×10^4 cells were seeded into each well of a 4-well plate (SPL Life Sciences, SPL-30004) in GM. After 2–3 days, when cells reached 90–100% confluence, the medium was replaced with differentiation medium (DM) consisting of DMEM supplemented with 2% horse serum (HS; Sigma, H1138) and 1× P/S. For extended differentiation culture (5 days), the DM was refreshed on day 3. For cell proliferation analysis, C2C12 myoblasts were seeded at a density of 4.0×10^4 cells per well in 4-well plates on control or VN-coated plates and cultured in DM. Cells were harvested at the indicated time points, and total cell numbers

View Article Online
DOI: 10.1039/D6BM00313C

were determined. Relative cell number per well was calculated by normalizing to the control condition.

Rat L6 myoblasts (a rat skeletal muscle–derived myoblast cell line) [20] were maintained in growth medium consisting of DMEM supplemented with 10% FBS without antibiotics, and cultured under standard conditions. For differentiation experiments, cells were seeded at a density of 1.0×10^5 cells per well in 4-well plates. Upon reaching approximately 80–90% confluence, the medium was replaced with differentiation medium consisting of DMEM supplemented with 2% HS without antibiotics, and cells were cultured for the indicated time periods. For cell proliferation analysis, L6 myoblasts were seeded at a density of 2.4×10^5 cells per well in 4-well plates and cultured in DM. Cells were harvested at the indicated time points (day 1 and day 2), and total cell numbers were determined. Relative cell number per well was calculated by normalizing to the control condition.

Human LHCN-M2 myoblasts (an immortalized human myoblast cell line) [21] were maintained in proliferation medium (MyoUp) consisting of DMEM and M199 (Thermo Fisher Scientific, 11150059) at a 4:1 ratio, supplemented with 15% FBS, 20 mM HEPES (Sigma-Aldrich, H0887), 3 µg/mL zinc sulfate (Sigma-Aldrich, Z0251), 1.4 µg/mL vitamin B12 (Sigma-Aldrich, V2876), 0.055 µg/mL dexamethasone (Sigma-Aldrich, D4902), 2.5 ng/mL recombinant human hepatocyte growth factor (HGF; PeproTech, 100-39H), and 5 ng/mL recombinant human basic fibroblast growth factor (bFGF;

View Article Online
DOI: 10.1039/D6BM00313C

PeproTech, 100-18B). For differentiation induction, LHCN-M2 cells were seeded at a density of 9.0 × 10^4 cells per well in 4-well plates and cultured until near confluence. The medium was then replaced with differentiation medium consisting of DMEM (FUJIFILM Wako, 043-30085) and M199 (Thermo Fisher Scientific, 11150059) at a 4:1 ratio, supplemented with 20 mM HEPES, 0.03 μg/mL zinc sulfate, 1.4 μg/mL vitamin B12, and 1× ITS-G supplement (Gibco, 41400045), and cells were cultured for the indicated time periods.

Cyclic RGDfV (cRGDfV) (SCP0111, Sigma-Aldrich) is an RGD-containing peptide antagonist with specificity for integrin αvβ3 and to inhibit binding to RGD-dependent ECM proteins such as vitronectin. In this study, cRGDfV was dissolved in dimethyl sulfoxide (DMSO) and used at a final concentration of 1 μM. DMSO was added at 0.04% (v/v) as a vehicle control.

For pharmacological inhibition of FAK, the selective FAK inhibitor PF-573228 (MedChemExpress, HY-10461) was added to the culture medium at final concentrations of 0.5 μM, determined to be non-toxic, at the time of differentiation induction. PF-573228 was dissolved in DMSO to prepare a stock solution and diluted into culture medium immediately before use. Control cultures received an equivalent volume of DMSO.

View Article Online
DOI: 10.1039/D6BM00313C

Pre-coating with Extracellular Matrix

Prior to cell seeding, culture wells were coated with the indicated ECM proteins at the desired coating density. Coated plates were incubated at 37 ℃ for 2 h, followed by aspiration of excess solution before use.

The following coating conditions were used for C2C12 myoblasts: fibronectin, 2.35 μg/cm^2 (FUJIFILM, 063-05591); vitronectin, 0.17–2.8 μg/cm^2 (FUJIFILM, 220-02041); laminin 511-E8 fragment (iMatrix-511, Nippi, 892011), 0.5 μg/cm^2; Matrigel, 2% (Corning, 354234); Gelatin, 0.2% gelatin (Sigma, G1890); and collagen type I, 0.2% (Nippi, ASC-1-100). Based on the optimization experiments (Supplementary Figures S2 and S4), the vitronectin coating density was set at 0.7 μg/cm^2 for serum-containing conditions and 1.4 μg/cm^2 for serum-free conditions.

For rat L6 and human LHCN-M2 myoblasts, vitronectin coating was applied at 0.7 μg/cm^2 and 1.4 μg/cm^2, respectively, based on optimization using cytotoxicity and maximal efficacy as criteria.

Immunofluorescence

Cells cultured in 4-well plates were fixed with freshly prepared 4% paraformaldehyde in Dulbecco's phosphate-buffered saline (PBS; FUJIFILM Wako, 041-20211) for 15 min at room temperature,

View Article Online
DOI: 10.1039/D6BM00313C

followed by permeabilization and blocking in PBS containing 1% Triton X-100 (FUJIFILM Wako, A16046), 1% BSA (Sigma, A3059), and 10% newborn calf serum (CS) (Biowest, S0750) for 1 h at room temperature. Cells were then incubated overnight at 4 ℃ with primary antibodies diluted in PBS containing 1% BSA, 1% CS, and 0.1% Triton X-100. Following three washes with PBS containing 0.1% Triton X-100 (PBST), cells were incubated for 2 h at room temperature or overnight at 4 °C with fluorophore-conjugated secondary antibodies diluted 1:500 in PBST containing 1% BSA and 1% CS. Nuclei were counterstained with DAPI (Sigma-Aldrich, D9542). After three washes with PBST, samples were kept in PBS and imaged. Fluorescence images were obtained using a BZ-X710 microscope (Keyence).

Antibodies for Immunofluorescence

Primary antibodies used were as follows: anti-Myosin Heavy Chain (MHC) (MF20, 1:500; R&D Systems, MAB4470), anti-Myogenin (1:500; abcam, ab124800), anti-phospho-Histone H3 (C-2, 1:1,000; Santa Cruz, sc-374669), anti-Cleaved Caspase-3 (Asp175) (5A1E, 1:500; Cell Signaling Technology, #9664), anti-Ki-67 (1:500; abcam, ab16667), anti-Vitronectin 65/75 (D-8, 1:250; Santa Cruz, sc-74484), and anti-phospho-FAK (Tyr397) (1:500; Cell Signaling Technology, #3283).

View Article Online
DOI: 10.1039/D6BM00313C

Secondary antibodies were goat anti-mouse IgG (H+L), Alexa Fluor 488 (abcam, ab150113); goat anti-mouse IgG (H+L), Alexa Fluor 594 (abcam, ab150116); and goat anti-rabbit IgG (H+L), Alexa Fluor 594 (abcam, ab150080).

Immunoblot analysis

Cells were lysed in SDS sample buffer containing 1M Tris-HCl (pH 6.8; FUJIFILM Wako, 015-20093), glycine (FUJIFILM Wako, 077-00735), 10% SDS (FUJIFILM Wako, 192-13981), 10 mg/mL bromophenol blue (BPB) (Nacalai Tesque, 05808-61), and β-mercaptoethanol (2-ME) (Nacalai Tesque, 21438-82). Protein concentration was determined using the Qubit Protein Assay Kit (Invitrogen, Q33211). Proteins were separated by SDS-PAGE using a 12% separating gel and a 4.5% stacking gel prepared from 30% (w/v) acrylamide/bis-acrylamide solution (29:1; FUJIFILM Wako , 015-25635), 1 M Tris-HCl (pH 8.8 for the separating gel, pH 6.8 for the stacking gel), 10% SDS, 10% (w/v) ammonium persulfate (APS; Nacalai Tesque, 02634-34), and TEMED (Nacalai Tesque, 33401-72). Electrophoresis was performed in 1× SDS running buffer, and proteins were transferred onto a PVDF membrane (MERCK, IPVH0010) using the HorizeBLOT 2M system (ATTO, WSE-4025) at 18 V/153 mA for 30 min. Membranes were blocked for 1 h at room temperature with either 0.3% skim

View Article Online
DOI: 10.1039/D6BM00313C

milk in TBST (TBS + 0.1% Tween-20) or EzBlock Chemi (ATTO, AE-1475). Membranes were then incubated overnight at 4 °C with primary antibodies diluted in Can Get Signal® Immunoreaction Enhancer Solution 1 (TOYOBO, NKB-101). Following three washes with TBST, membranes were incubated with HRP-conjugated secondary antibodies diluted 1:10,000 in Can Get Signal® Immunoreaction Enhancer Solution 2 (TOYOBO, NKB-101) for 3 h at room temperature or overnight at 4 °C. Signals were detected using ECL reagents as follows: Start (Cytiva, RPN3243), Prime (Cytiva, RPN2232), and Select (Cytiva, RPN2235) and visualized using a LuminoGraph I imaging system (ATTO, WSE-6100). Molecular weights were verified using the EzProtein Ladder (ATTO, WSE-7020).

To compare vitronectin abundance among different serum sources, FBS, adult bovine serum (ABS) (B9433, Sigma-Aldrich), and HS were analyzed by immunoblotting. Each serum sample was normalized by total protein content, and 1 μg of total protein from each serum was loaded.

Antibodies for Immunoblot Analysis

Primary antibodies used were as follows: anti-MyoD (5.8A, 1:5,000; Novus Biologicals, NB100-56511), anti-Myogenin (1:10,000; abcam, ab124800), anti-MHC (MF20, 1:5,000; R&D Systems,

View Article Online
DOI: 10.1039/D6BM00313C

MAB4470), anti-β-Actin (C4, 1:5000; Santa Cruz, sc-47778), anti-Stat3 (D3Z2G, 1:5,000; Cell Signaling Technology, #12640), anti-phospho-Stat3 (Tyr705, D3A7, 1:5,000; Cell Signaling Technology, #9145), anti-ERK1/2 (C-9, 1:5,000; Santa Cruz, sc-514302), anti-phospho-ERK (E-4, 1:5,000; Santa Cruz, sc-7383), anti-p38α/β MAPK (A-12, 1:5,000; Santa Cruz, sc-7972), anti-phospho-p38 (E-1, 1:5,000; Santa Cruz, sc-166182), anti-p21 Waf/Cip1 (F-5, 1:5,000; Santa Cruz, sc-6246), anti-p27 Kip1 (F-8, 1:5,000; Santa Cruz, sc-1641), anti-FGF Receptor 1 (D8E4, 1:5,000; Cell Signaling Technology, #9740), anti-p-FGF Receptor 1 (Tyr653/654) (D4X3D, 1:5,000; Cell Signaling Technology, #52928), anti-Insulin Receptor β (4B8, 1:5,000; Cell Signaling Technology, #3025), anti-p-IGF-1 Receptor β (Tyr1135/1136)/Insulin Receptor β (Tyr1150/1151) (19H7, 1:5,000; Cell Signaling Technology, #3024), anti-Vitronectin 65/75 (D-8, 1:5,000; Santa Cruz, sc-74484), anti-FAK (1:5,000; Cell Signaling Technology, #3285), and anti-phospho-FAK (Tyr397) (1:5,000; Cell Signaling Technology, #3283).

Secondary antibodies were anti-mouse IgG (H+L chain), pAb-HRP (MBL, 330); and anti-rabbit IgG (H+L chain), pAb-HRP (MBL, 458).

RNA Preparation and Real-Time PCR

View Article Online
DOI: 10.1039/D6BM00313C

Total RNA was extracted using RNeasy Mini Kit (QIAGEN, 74104) according to the manufacturer's instructions. cDNA was synthesized using the ReverTra Ace qPCR RT Master Mix (TOYOBO, FSQ-201). Real-time PCR was performed using THUNDERBIRD SYBR qPCR Mix (TOYOBO, QPS-201) on a Mic qPCR Cycler (Bio Molecular Systems). Gene expression levels were normalized to mouse *Hprt* expression and calculated using the comparative CT (ΔΔCt) method. Primer sequences were as follows:

Hprt-F (CAGTCCCAGCGTCGTGATTA), *Hprt*-R (AGCAAGTCTTTCAGTCCTGTC), *Vitronectin*-F (CCCCTGAGGCCCTTTTTCATA), *Vitronectin*-R (CAAAGCTCGTCACACTGACA).

Immunodepletion of Vitronectin from FBS

rProtein A Sepharose™ Fast Flow beads (Cytiva, 17127901) were gently rotated for 2 h at room temperature to ensure homogeneous suspension. A 100 µL aliquot of beads was washed once with KMH buffer (100 mM KCl [FUJIFILM Wako, 169-03542], 2.5 mM $MgCl_2$ [FUJIFILM Wako, 135-00165], and 20 mM HEPES-KOH [pH 7.5; Nacalai Tesque, 15639-84]) by centrifugation (300 × g, 5 min).

View Article Online
DOI: 10.1039/D6BM00313C

Beads were then incubated with 10 μL of anti-vitronectin 65/75 antibody (D-8; Santa Cruz, sc-74484) and control antibody (Santa Cruz, sc-3877) overnight at 4 ℃. Following two washes with KMH buffer (300 × g, 5 min), 200 μL of FBS (Gibco, 10270-106) was added to the antibody-bound beads, and the mixture was rotated overnight at 4 ℃. The supernatant was collected and filtered through a 0.2 μm membrane filter (Advantec, 13CP020AS) to obtain vitronectin-depleted FBS and control FBS.

Culture in Serum-Free Medium

The detailed composition of the serum-free media used, including DA-X, is described below. The DA-X medium [22], a fully serum-free medium used in this study, was based on DMEM (high glucose) with L-glutamine, phenol red, and sodium pyruvate (FUJIFILM Wako, 043-30085), supplemented with Insulin–Transferrin–Selenium–Ethanolamine (ITS-X) (1×; Gibco, 51500056), bovine serum albumin (BSA) (5 mg/mL; Sigma, A3059), L-glutamine (2 mM; FUJIFILM Wako, 073-05391), and penicillin–streptomycin mixed solution (1×; FUJIFILM Wako, 168-23191).

Where indicated, leukemia inhibitory factor (LIF) was supplied at 0.1% (v/v) using conditioned medium derived from COS cells transiently transfected with a LIF expression vector (see below). In addition, water-soluble cholesterol was added to the medium at a final concentration of 10 μM, and β-

View Article Online
DOI: 10.1039/D6BM00313C

mercaptoethanol (2-ME) (Nacalai Tesque, 21438-82) was added at a final concentration of 100 μM [23]. All medium components were pre-mixed and stored at 4 °C. However, the water-soluble cholesterol solution was added freshly immediately before use to prevent crystallization in the pre-mixed medium. The preparation of water-soluble cholesterol is described below. For selected experiments, vitronectin was coated at a density of 1.4 μg/cm², and recombinant human IGF-1 (2 ng/mL; PeproTech, #100-11) and FGF-2 (100 ng/mL; PeproTech, #100-18B) were added as indicated.

Preparation of LIF-Conditioned Medium

LIF-conditioned medium was prepared from COS cells transiently transfected with the pCAGGS–LIF expression vector [24]. Briefly, COS cells were seeded in 10-cm dishes and cultured to approximately 70–80% confluence, followed by transfection using Lipofectamine 3000 (Thermo Fisher Scientific) according to the manufacturer's instructions. On the following day, transfected cells were detached with trypsin and passaged at approximately a 1:4 dilution into four new 10-cm dishes. Culture supernatants were collected and filtered through a 0.22-μm membrane filter on day 3 and day 4, after which the cells were discarded. The collected supernatants were stored at −20 °C and used as a source of LIF in serum-free cultures.

View Article Online
DOI: 10.1039/D6BM00313C

Importantly, stable proliferation and maintenance of undifferentiated morphology were observed across a range of 0.1–0.2% (v/v), whereas lower concentrations led to partial spontaneous differentiation, as evidenced by the appearance of myotube-like structures (Figure S7). This phenotype may serve as a practical indicator for assessing batch quality of conditioned medium. Based on functional validation experiments, a concentration of 0.1% (v/v) was used as the standard condition for serum-free culture throughout this study.

Preparation of Water-Soluble Cholesterol Solution

For the preparation of a 50 mM cholesterol/EtOH stock solution, 19.3 mg of cholesterol (Sigma, C8667) was dissolved in 1 mL of 100% EtOH by incubation at 80 °C. For water-solubilization of the cholesterol/EtOH solution, 42 mg of Methyl-β-cyclodextrin (Sigma-Aldrich, 332615) was added to the 1 mL of 5 mM cholesterol/EtOH solution. The solution was stored at −20 °C before use.

Rotary suspension spheroid culture

Cells were seeded at a density of 6.0×10^3 cells per well in a 96-well U-bottom plate (Thermo Fisher Scientific, 174925) and incubated for one day in 100 μL of GM. On the following day, the formed

View Article Online
DOI: 10.1039/D6BM00313C

spheroids were carefully transferred using a MICROCAPS pipette (Drummond, 1-000-0500) under a stereomicroscope to a 4-well plate (SPL Life Sciences, SPL-30004) containing 500 µL of DM. The plates were rotated at 150 rpm on a rotary shaker (Waken B TECH, WB-T101SRC). After completing the immunofluorescence staining, the spheroids were transferred to APS-coated glass slides (MATSUNAMI, SAPS-01), and excess PBST was carefully removed. The spheroids were then mounted in VECTASHIELD mounting medium (Vector, H-1200). The slides were then covered with NEO cover glass (MATUNAMI, C024501) and sealed with a nail topcoat. Images were acquired using a fluorescence microscope (Keyence, BZ-X710) and a confocal laser scanning microscope (Olympus, FV-3000).

Primary Culture of Embryonic Chick Myogenic Cells

As described previously [25], fertilized chicken eggs obtained from a certified poultry supplier were incubated for 10 days, and thigh muscle tissue was dissected from embryos using fine forceps. The femurs were surgically removed, and the isolated muscle tissue was finely minced and washed twice with PBS. The minced tissue was then digested in HBSS (Nacalai Tesque, 09735-75) containing 2 mg/mL collagenase type II (Worthington Biochemical Corporation, WOR-CLS2) at 37 °C for 40–60

View Article Online
DOI: 10.1039/D6BM00313C

min, with gentle pipetting every 10–15 min to facilitate cell dissociation. The resulting cell suspension was filtered through a 40 μm cell strainer (Corning, 431750) to obtain single cells. Approximately 5.0 × 10^5 cells were seeded in GM per well in 4-well plates pre-coated with either 0.2% gelatin (control) or 0.7 μg/cm² vitronectin (VN) to ensure stable attachment. On the following day, the medium was replaced with DM, and cells were induced to differentiate for approximately 6 h. Cultured embryonic chick myogenic cells were then subjected to subsequent analyses. All animal experiments were conducted in accordance with the ethical guidelines of Kindai University and were reviewed and approved by the Kindai University Animal Care and Use Committee.

Statistical analysis

Statistical analyses were performed using unpaired two-tailed Student's t-test for comparisons between two groups. For experiments involving three or more groups, one-way ANOVA followed by Tukey's multiple comparisons test was applied. Growth curve analyses were evaluated using two-way ANOVA. A p value < 0.05 was considered statistically significant.

Results:

View Article Online
DOI: 10.1039/D6BM00313C

| Vitronectin suppresses myogenic differentiation of C2C12 cells

C2C12 myoblasts proliferate robustly under growth medium (GM; DMEM supplemented with 10% FBS), whereas switching to differentiation conditions (DM; DMEM supplemented with 2% HS) rapidly induces myogenic differentiation characterized by cell fusion and the induction of myotube-associated markers (Figure 1a). While several extracellular matrix (ECM) components present in FBS, including fibronectin, collagen, and laminin, have been extensively studied and are generally recognized to support myoblast adhesion and differentiation, the functional contribution of vitronectin (VN) to myogenic regulation remains poorly defined.

To examine the role of VN, C2C12 myoblasts were cultured on plates coated with fibronectin, vitronectin, laminin, collagen type I, Matrigel, or gelatin (Figure S1). Gelatin was included as a commonly used nonspecific adhesion substrate, whereas Matrigel served as a complex basement membrane–like ECM reference.

Under differentiation conditions, cells cultured on uncoated plates as a control or on fibronectin-, laminin-, Matrigel-, collagen-, or gelatin-coated surface exhibited typical myogenic morphology, including extensive myotube formation and abundant MHC-positive cells (Figure S1). In contrast, cells cultured on VN-coated plates showed a marked reduction in myogenin- and MHC-positive cells

View Article Online
DOI: 10.1039/D6BM00313C

in a coating-density-dependent manner (Figure 1b, c; Figures S1, S2). Consistently, VN-cultured cells displayed a reduced fusion index and remained predominantly mononuclear (Figure 1d).

Immunoblot analysis further revealed that the expression of key myogenic regulators, including MyoD, myogenin, and MHC, was significantly decreased under VN conditions (Figure 1e). Moreover, phosphorylation of signal pathways implicated in myogenic progression, including STAT3 [26–28], ERK1/2 [29,30], and p38 MAPK [29,31], was attenuated in cells cultured on VN (Figure 1f). Together, these observations indicate that VN suppresses both the morphological and signaling events required for myogenic differentiation.

Vitronectin is known to interact primarily with integrin αvβ3, which mediates adhesion-dependent signaling across multiple cell types [3]. To determine whether integrin αvβ3 contributes to the VN-dependent inhibition of differentiation, we examined the effects of the competitive αvβ3 antagonist peptide cRGDfV [3,32]. C2C12 myoblasts were cultured under differentiation conditions on either uncoated or VN-coated plates in the presence or absence of cRGDfV.

Immunostaining for MHC demonstrated that the suppression of myotube formation observed on VN-coated plates was significantly rescued by cRGDfV treatment (Figure 1g). Notably, cRGDfV alone modestly increased the proportion of MHC-positive cells under control conditions, suggesting

View Article Online
DOI: 10.1039/D6BM00313C

that basal αvβ3 signaling partially restrains differentiation. Quantitative analysis of the fusion index confirmed both the rescue effect in the VN plus cRGDfV group and the enhancement observed with cRGDfV alone (Figure 1h).

Collectively, these findings support a model in which VN suppresses myogenic differentiation through integrin αvβ3-dependent signaling.

| Vitronectin enhances myoblast proliferation and survival by sustaining growth factor signaling and preventing cell cycle exit

Since VN markedly inhibited myogenic differentiation, we next examined whether this effect was associated with altered proliferative behavior of C2C12 myoblasts. Proliferation and terminal differentiation are widely considered mutually exclusive cellular programs, such that conditions suppressing differentiation often preserve proliferative capacity [33–35].

To directly assess proliferation under differentiation conditions, C2C12 cells were seeded at low density in DM (Figure 2a), thereby minimizing the confounding effects of density-dependent growth arrest typically observed in standard differentiation protocols. Cell counting revealed a significant increase in total cell number on VN-coated plates compared with uncoated controls, in a coating-

View Article Online
DOI: 10.1039/D6BM00313C

density-dependent manner (Figure 2b; Figures S1b, S2c).

To determine whether this increase reflected enhanced cell division, we performed immunofluorescence staining for phosphorylated histone H3 (p-Histone H3), a well-established mitotic marker. The proportion of pH3-positive cells was significantly elevated under VN-coated conditions (Figure 2c), indicating increased mitotic activity.

We next examined whether VN influences cell survival, as apoptotic processes can accompany myogenic progression under differentiation conditions [36]. Immunostaining for cleaved caspase-3 demonstrated a pronounced reduction in apoptotic cells on VN-coated substrates (Figure 2d), suggesting that VN promotes not only cell division but also survival.

Because cell cycle withdrawal is a prerequisite for myogenic differentiation, we investigated whether VN affects the expression of cell cycle regulators. Immunoblot analysis revealed that the cyclin-dependent kinase inhibitors p21 [37,38] and p27 [39] were downregulated in cells cultured on VN (Figure 2e), consistent with suppression of cell cycle exit.

This finding suggests that VN suppresses cell cycle arrest, thereby maintaining the proliferative capacity of myoblasts even under differentiation conditions.

To explore the signaling basis of these effects, we assessed the activation state of growth factor

View Article Online
DOI: 10.1039/D6BM00313C

receptors known to regulate myoblast proliferation. Insulin-like growth factor receptor (IGFR) signaling [40,41] and fibroblast growth factor receptor (FGFR) signaling [10,42] are key modulators of myoblast growth and differentiation. Notably, both receptors exhibited increased phosphorylation under VN-coated conditions (Figure 2f), indicating sustained activation of growth factor–associated pathways.

Collectively, these findings indicate that VN enhances myoblast proliferation by increasing mitotic activity, reducing apoptosis, suppressing cell cycle inhibitors, and maintaining growth factor receptor signaling under differentiation conditions.

| Vitronectin supports proliferative expansion and prevents premature differentiation of myoblast spheroids in three-dimensional culture

Three-dimensional (3D) spheroid and organoid culture systems are widely used to recapitulate tissue-like architecture in vitro. A persistent challenge in these systems is that aggregate growth is inherently constrained: as spheroids enlarge, diffusion limitations and insufficient mass transport frequently lead to hypoxic or necrotic cores, thereby restricting further expansion and functional maturation [43,44]. In myogenic models, an additional limitation arises from the tendency of myoblasts to undergo rapid

View Article Online
DOI: 10.1039/D6BM00313C

differentiation upon establishment of extensive cell–cell contact, which further limits proliferative expansion of 3D constructs [45].

To examine whether VN modulates myoblast behavior in a 3D context, we employed a suspension-based spheroid culture system (Figure 3). C2C12 myoblasts were seeded into 96-well U-bottom plates and allowed to self-aggregate for one day under differentiation conditions. The resulting spheroids were then transferred to 4-well plates and maintained under rotary suspension culture (Figure 3a).

In contrast to the substrate-coating strategy used in two-dimensional experiments, VN was directly supplemented into the culture medium to ensure uniform exposure throughout the spheroid structure. Under VN-treated conditions, spheroids exhibited a significant increase in total cell number relative to controls (Figure 3b) and a marked enlargement of spheroid size (Figure 3c).

Phase-contrast imaging and DAPI staining confirmed the formation of enlarged aggregates. Notably, immunofluorescence analysis revealed substantially reduced expression of the differentiation marker MHC in VN-treated spheroids (Figure 3c). Confocal microscopy further demonstrated diminished MHC signals accompanied by increased expression of the proliferation marker Ki-67 (Figure 3d).

Collectively, these observations indicate that VN suppresses premature myogenic differentiation while promoting proliferative expansion of myoblast spheroids in 3D culture, consistent with its effects

View Article Online
DOI: 10.1039/D6BM00313C

observed in two-dimensional systems. These findings suggest that VN-mediated matrix signaling may provide a strategy to sustain proliferative capacity and overcome intrinsic size limitations associated with myogenic spheroid models.

| Serum-derived vitronectin regulates myoblast proliferation and differentiation

Because vitronectin (VN) suppressed myogenic differentiation and promoted proliferative behavior (Figures 1–3), we next examined whether serum-dependent variation in VN abundance contributes to myoblast state regulation. Serum replacement from fetal bovine serum (FBS) to horse serum (HS) is a canonical trigger for C2C12 differentiation, yet the extracellular determinants underlying this transition remain incompletely defined.

Immunoblot analysis revealed that VN was abundantly present in FBS but was nearly undetectable in HS (Figure 4a). Notably, VN abundance was also substantially lower in adult bovine serum (ABS) relative to FBS (Figure 4a; Figure S3), indicating that VN content varies markedly among serum types.

Following differentiation induction, VN levels decreased sharply by day 1 (Figure 4b), a trend confirmed by immunofluorescence analysis showing reduced extracellular VN signals under differentiation conditions (Figure 4c). qPCR analysis demonstrated that VN transcript levels remained

View Article Online
DOI: 10.1039/D6BM00313C

low and did not parallel protein abundance (Figure 4d), supporting the interpretation that VN present under growth conditions is predominantly serum-derived.

To directly assess the functional significance of serum-derived VN, VN was selectively removed from FBS by immunodepletion. VN-depleted FBS significantly enhanced myotube formation under reduced-serum conditions (5% FBS) (Figure 4e, f), demonstrating that serum-associated VN levels influence differentiation efficiency.

Because VN promoted proliferation under differentiation conditions (Figure 2), we next examined whether VN–integrin signaling contributes to proliferative maintenance under growth conditions. Long-term culture experiments performed in GM revealed that continuous inhibition of integrin αvβ3 signaling by cRGDfV suppressed cell expansion relative to controls (Figure 4g).

Given that cRGDfV competitively inhibits αvβ3–RGD interactions, this result is consistent with a model in which serum-derived VN supports sustained myoblast proliferation under serum-containing growth conditions.

| Vitronectin and LIF establish a serum-free proliferative state

We next investigated whether VN could functionally replace serum to sustain myoblast proliferation

View Article Online
DOI: 10.1039/D6BM00313C

under defined serum-free conditions. Using the previously established DA-X serum-free medium [22], we evaluated the capacity of VN to support long-term C2C12 expansion.

Because serum provides a complex mixture of survival and anti-differentiation cues, its removal typically leads to growth arrest, spontaneous differentiation, and increased cell death in myoblasts (Figure 4h). Previous studies have shown that leukemia inhibitory factor (LIF) suppresses myogenic differentiation and apoptosis while preserving proliferative capacity without acting as a classical mitogen [46,47].

Consistent with this framework, VN alone was insufficient to maintain stable growth under serum-free conditions (Figures S4). In contrast, co-administration of LIF-conditioned medium enabled robust survival and sustained proliferation, allowing cells cultured on VN-coated surfaces to continue proliferating while resisting differentiation (Figures 4h and S4). Notably, proliferation was maintained even in the absence of canonical mitogens such as FGF-2 and IGF-1, indicating that VN together with LIF establishes a proliferation-permissive extracellular environment that does not strictly depend on exogenous growth factor supplementation. Addition of FGF-2 or IGF-1 further enhanced proliferation (Figure S4d), suggesting that this system provides a modular proliferative baseline.

Importantly, cells expanded for multiple passages under VN/LIF serum-free conditions retained

View Article Online
DOI: 10.1039/D6BM00313C

myogenic competence (Figure S5), maintained MyoD expression, and efficiently differentiated upon transfer to HS-containing medium (DM). Among the tested conditions, only the cholesterol-only medium exhibited reduced differentiation efficiency. Furthermore, when compared with alternative ECM substrates, VN consistently supported the most robust proliferative response (Figure S6), highlighting its unique capacity to sustain myoblast expansion in defined serum-free environments.

| Vitronectin exerts conserved effects on myogenic differentiation and proliferation across species

To evaluate whether the effects of VN are conserved across species, we extended our analysis to additional myoblast models. In rat L6 myoblasts [20], VN similarly suppressed myogenic differentiation, as evidenced by reduced proportions of myogenin- and MHC-positive cells and decreased fusion index (Figure 5a–b). In parallel, VN significantly enhanced proliferative activity under differentiation conditions (Figure 5c). We further examined human LHCN-M2 myoblasts [21], where VN also inhibited myogenic differentiation, as indicated by decreased differentiation index and fusion index (Figure 5d–e). Proliferation analysis was not performed in LHCN-M2 cells, as this immortalized cell line may not fully reflect physiological proliferative responses compared with non-transformed myoblast models

View Article Online
DOI: 10.1039/D6BM00313C

such as C2C12 and L6 cells.

These results demonstrate that the differentiation-suppressive and proliferation-promoting effects of VN are conserved across species and are observed in both rodent and human myoblast systems.

| Vitronectin promotes proliferation and suppresses myogenic differentiation in primary avian embryonic myoblasts

Given that the differentiation-suppressive and proliferation-promoting effects of vitronectin (VN) were conserved across multiple myoblast cell lines (Figure 5), we next sought to validate these findings in primary skeletal muscle cells. To address this question, primary myogenic cells were isolated from the thigh muscles of 10-day-old chicken embryos (Figure 6a). In contrast to immortalized C2C12 cells, primary embryonic myoblasts exhibit differentiation rapidly and frequently contain pre-fused myotubes at the time of plating, which limits the feasibility of long-term proliferation assays. Therefore, short-term differentiation experiments were performed using a 6-hour induction period.

To evaluate the influence of VN on myogenic progression, the fusion index was quantified by measuring the number of nuclei per myotube. After 6 hours of differentiation, the number of nuclei per myotube was significantly reduced under VN-supplemented conditions compared with controls

View Article Online
DOI: 10.1039/D6BM00313C

(Figure 6b), indicating suppression of myotube formation.

Consistent with this observation, total cell counts revealed a significant increase in cell number in the presence of VN (Figure 6c). Immunofluorescence staining for the mitotic marker phosphorylated histone H3 (p-Histone H3) further demonstrated an increased proportion of p-Histone H3–positive cells under VN conditions (Figure 6d), indicating elevated mitotic activity. Moreover, in three-dimensional suspension culture, VN supplementation similarly increased total cell number within spheroids derived from chicken embryonic myogenic cells (Figure 6e).

Collectively, these findings indicate that the proliferation-promoting and differentiation-suppressive effects of VN are conserved across species and are not restricted to immortalized murine cell lines.

Discussion:

The present study identifies vitronectin (VN) as an extracellular matrix component that actively suppresses myogenic differentiation while sustaining proliferative capacity in myoblasts. Although ECM proteins have traditionally been viewed as permissive substrates that support differentiation, our findings demonstrate that specific matrix components can instead impose a differentiation-restrictive state, thereby stabilizing a proliferative cellular phenotype.

View Article Online
DOI: 10.1039/D6BM00313C

A central mechanistic question concerns how VN-mediated signaling interferes with differentiation-associated pathways. In our system, VN exposure attenuated phosphorylation of STAT3, ERK1/2, and p38 MAPK, signaling axes widely implicated in myogenic progression [27,30,48–50]. Integrin-mediated signaling is classically transduced through focal adhesion kinase (FAK)–Src signaling complexes [51,52], which link integrin engagement to intracellular signaling pathways. Notably, we did not observe appreciable changes in FAK activation, as assessed by phosphorylation at Tyr397, nor did pharmacological inhibition of FAK rescue the VN-induced suppression of differentiation (Figure S8). These findings suggest that canonical FAK-dependent integrin signaling is not a major mediator of VN function in this system.

This observation is notable because integrin αvβ3 signaling is commonly interpreted through canonical FAK–Src pathways. Our results therefore suggest that VN establishes a differentiation-restrictive state through a non-canonical signaling mechanism, rather than through classical adhesion-associated kinase activation. While the potential involvement of Src family kinases cannot be excluded, this remains a subject for future investigation. Accordingly, the attenuation of STAT3, ERK1/2, and p38 signaling is interpreted not as a direct downstream effect of VN–integrin engagement, but rather as a secondary consequence of the altered cellular state under VN conditions.

View Article Online
DOI: 10.1039/D6BM00313C

Despite this mechanistic ambiguity, at least two non-mutually exclusive explanations may account for the observed effects. First, integrin-dependent signaling downstream of VN may influence intracellular signaling through FAK-independent pathways [53–55]. Second, VN-mediated maintenance of cell-cycle progression may indirectly suppress differentiation, as withdrawal from the cell cycle is a prerequisite for myogenic commitment. These cell cycle–related findings support the established incompatibility between proliferative expansion and terminal differentiation in myogenic cells, suggesting that VN stabilizes a proliferation-permissive state that functionally antagonizes differentiation programs.

Consistent with this interpretation, VN was associated with sustained phosphorylation of growth factor receptors, including IGF-1R and FGFR, under differentiation conditions (Figure 2f). Integrin-mediated adhesion is known to influence receptor organization and signaling persistence at the plasma membrane, providing a conceptual framework for ECM-dependent modulation of growth factor responsiveness [3,4,19,56]. In this context, integrin–growth factor receptor cross-talk provides a plausible mechanism by which VN sustains proliferative signaling independently of canonical FAK pathways [51,57]. Rather than acting as a classical soluble mitogen, VN may contribute to the stabilization of membrane-associated signaling microenvironments that prolong receptor activity even when growth

View Article Online
DOI: 10.1039/D6BM00313C

factor availability is reduced.

The functional consequences of VN were particularly evident in three-dimensional spheroid culture, where VN promoted aggregate expansion while limiting premature differentiation (Figures 3 and 6e). Diffusion constraints and early lineage commitment represent intrinsic barriers to spheroid enlargement in myogenic systems [58–60]. Our observations suggest that VN-rich extracellular environments help preserve proliferative capacity within 3D constructs, thereby enabling more effective expansion of myogenic cell populations prior to differentiation. These findings support the relevance of VN-mediated microenvironmental regulation in more complex three-dimensional systems.

Importantly, our data also suggest a revised interpretation of the classical serum-switch paradigm in myogenic differentiation (Figure 1a). Replacement of fetal bovine serum with horse serum has long been considered to induce differentiation primarily through withdrawal of soluble mitogenic factors [6,9]. However, our results demonstrate that vitronectin is abundant in FBS but markedly reduced in HS, and that depletion of serum-derived VN enhances differentiation efficiency (Figure 4). These findings indicate that changes in ECM composition, rather than solely soluble factors, play a critical role in regulating myoblast state transitions. These results establish matrix composition as an active determinant of cell fate, operating in parallel with soluble mitogenic signals.

View Article Online
DOI: 10.1039/D6BM00313C

The functional relevance of VN was further supported by its conserved effects across multiple myoblast systems. VN suppressed differentiation and promoted proliferation not only in C2C12 cells but also in rat L6 and human LHCN-M2 myoblasts (Figure 5), as well as in primary embryonic chicken myogenic cells (Figure 6). These results demonstrate that the differentiation-restrictive function of VN is broadly conserved across species and experimental contexts. In addition, the lack of overt cytotoxicity in primary myogenic cells (Figure 6) and the established use of vitronectin in human pluripotent stem cell culture systems [61,62] further support its biological compatibility across multiple cell types.

In addition, we established a defined serum-free culture system in which VN cooperates with leukemia inhibitory factor (LIF) to support myoblast expansion (Figures 4h and S4). LIF alone is not sufficient to drive proliferation, but instead functions to suppress differentiation and support cell survival. In this system, VN and LIF appear to act cooperatively, with VN providing adhesion-dependent proliferative support and LIF suppressing differentiation-associated cell cycle exit in a dose-dependent manner (Figure S7). Notably, sustained proliferation was observed even in the absence of canonical mitogens such as FGF-2 and IGF-1, indicating that VN establishes a proliferation-permissive extracellular environment. Supplementation with FGF-2 and IGF-1 further enhanced proliferation,

View Article Online
DOI: 10.1039/D6BM00313C

suggesting that VN does not replace growth factor signaling, but rather supports and stabilizes growth factor–dependent signaling inputs. Collectively, this system enables sustained expansion under defined conditions while preserving differentiation competence, providing a controllable platform for serum-free myoblast culture.

In this context, vitronectin can be viewed not merely as an adhesion substrate, but as a matrix component that actively stabilizes a proliferation-permissive and differentiation-restrictive cellular state. This property distinguishes VN from conventional ECM substrates that are typically associated with differentiation support (Figure S1).

Nevertheless, several limitations should be noted. First, the precise molecular pathways linking VN–integrin αvβ3 engagement to downstream signaling remain to be fully elucidated, particularly with respect to potential involvement of Src family kinases and other non-canonical integrin signaling pathways. Second, while cross-species validation was performed using multiple cell lines and primary cells, further validation in additional primary human systems will be required to fully establish physiological relevance.

Taken together, our findings identify vitronectin as a key ECM component that enforces a differentiation-restrictive microenvironment and highlight the importance of matrix composition in

View Article Online
DOI: 10.1039/D6BM00313C

regulating myoblast fate. These insights provide a conceptual basis for engineering ECM-based systems to control progenitor cell expansion and differentiation in regenerative and biomaterials applications.

Author contributions:

TK: Data curation, Investigation, Methodology, Project administration, Writing–original draft. AM,YT, MH, and KM: Investigation, Methodology. YC: Data curation, Writing–original draft. DO: Conceptualization, Funding acquisition, Investigation, Methodology, Project administration, Resources, Writing–original draft, Writing–review and editing. All authors participated in drafting and revising the manuscript. All authors contributed to the article and approved the version submitted for publication.

Funding:

This work was supported by grants from Kindai University Research Enhancement Grant (IP003), the Ito Foundation, and the Urakami Foundation for Food and Food Culture Promotion (DO). TK was supported by the Sasakawa Scientific Research Grant from the Japan Science Society.

View Article Online
DOI: 10.1039/D6BM00313C

Acknowledgments:

We would like to thank Prof. Yoko Kato (Kindai Univ.) for the valuable comments and Jafar Sharif (Laboratory for Developmental Genetics, RIKEN Center for Integrative Medical Sciences (IMS)) for the kindly gifted materials.

Conflict of interest

The authors declare that the research was conducted in the absence of any commercial or financial relationship that could be construed as a potential conflict of interest.

Figure captions

Figure 1 | Inhibitory effects of vitronectin on myogenic differentiation in mouse C2C12 myoblasts.

a, Schematic representation of myogenic differentiation in C2C12 myoblasts and the expression dynamics of representative differentiation markers. Myoblast proliferation is maintained in growth medium (GM; DMEM supplemented with 10% fetal bovine serum (FBS)), whereas differentiation

View Article Online
DOI: 10.1039/D6BM00313C

medium (DM; DMEM supplemented with 2% horse serum (HS)) induces rapid differentiation into multinucleated myotubes. **b,** Representative phase-contrast and immunofluorescence images showing myogenin expression on day 3 in DM. White arrowheads indicate representative differentiating myotubes. The differentiation index, quantified as the proportion of myogenin-positive cells relative to total nuclei, is shown in the graph (Control: n = 1652; Vitronectin: n = 1746). **c,** Time-course analysis of myotube formation by immunofluorescence for myosin heavy chain (MHC). **d,** Fusion index quantified as the number of nuclei per MHC-positive myotube on day 3 in DM (Control: n = 50; Vitronectin: n = 50). Numbers shown in the images indicate nuclei within representative myotubes. **e,** Immunoblot analysis of MyoD, myogenin, and MHC. **f,** Immunoblot analysis of total and phosphorylated STAT3, ERK1/2, and p38 MAPK. **g-h**, Immunofluorescence analysis of MHC expression after 3 days in DM under the indicated conditions. Quantification shows the differentiation index (g) and fusion index (h). β-ACT was used as a loading control. Scale bar: 100 μm. Nuclei were counterstained with DAPI. Data are presented as mean ± s.d. Statistical significance was determined using Student's t-test (**$p < 0.01$).

Figure 2 | Vitronectin promotes proliferation of C2C12 myoblasts under differentiation

View Article Online
DOI: 10.1039/D6BM00313C

conditions

a, Schematic representation of the experimental design for assessing proliferative responses under low-density DM conditions. **b,** Representative DAPI-stained nuclei images and relative cell numbers on day 3 (n = 6). **c,** Representative immunofluorescence images for phospho-histone H3 (p-Histone H3) and quantification of positive cells (Control: n = 1345; Vitronectin: n = 2632). **d,** Representative immunofluorescence images for cleaved caspase-3 (Control: n = 2499; Vitronectin: n = 2345). **e,** Immunoblot analysis of p21 and p27. **f,** Immunoblot analysis of total and phosphorylated IGF-1R and FGFR. β-ACT was used as a loading control. Scale bar: 100 μm. White arrowheads indicate representative positive cells. Data are presented as mean ± s.d. Statistical significance was determined using Student's t-test (**$p < 0.01$, *$p < 0.05$).

Figure 3 | Vitronectin enhances proliferation and suppresses differentiation in rotary suspension spheroid culture

a, Schematic representation of the rotary suspension spheroid culture system. **b,** Quantification of total cell numbers per spheroid on day 6 (n = 5). **c,** Representative phase-contrast and immunofluorescence images of spheroids stained for MHC and DAPI. **d,** Representative confocal images showing MHC,

View Article Online
DOI: 10.1039/D6BM00313C

Ki-67, and DAPI. Quantification of positive cells is shown in the graphs. Scale bars: 100 μm (c), 50 μm (d). Data are presented as mean ± s.d. Statistical significance was determined using Student's t-test (**$p < 0.01$).

Figure 4 | Serum-derived vitronectin regulates myoblast differentiation and proliferation

a, Immunoblot analysis of VN protein levels in FBS, adult bovine serum (ABS), and HS. **b,** Immunoblot analysis of VN protein following differentiation induction. β-ACT was used as a loading control. **c,** Representative immunofluorescence images showing VN localization. **d,** qPCR analysis of VN transcript levels (n = 3). **e,** Immunoblot confirmation of VN immunodepletion. **f,** Quantification of differentiation efficiency using control and VN-depleted FBS. **g,** Long-term proliferation analysis over 24 days (7 passages) in GM with or without the integrin αvβ3 inhibitor cRGDfV, quantified as cumulative cell number. **h,** Representative phase-contrast images of C2C12 cells cultured in GM, DM, and a serum-free DA-X medium supplemented with LIF on plates coated with or without VN coating. Images were captured on day 5 in each condition. Scale bar: 100 μm. Data are presented as mean ± s.d. Statistical significance was determined using one-way ANOVA (d) and Student's t-test (f) (*$p < 0.05$).

View Article Online
DOI: 10.1039/D6BM00313C

Figure 5 | Conserved effects of vitronectin on myogenic differentiation and proliferation across species

a, Representative immunofluorescence images showing myogenin and MHC expression in rat L6 myoblasts cultured under differentiation conditions on control or VN-coated substrates. Quantification of myogenin- and MHC-positive cells relative to total nuclei is shown (Control: n = 725; Vitronectin: n = 71 for myogenin; Control: n = 888; Vitronectin: n = 216 for MHC). **b,** Representative immunofluorescence images of MHC and DAPI staining in L6 myoblasts. Fusion index, defined as the number of nuclei per MHC-positive myotube, is quantified in the graph. **c,** Relative cell numbers of L6 myoblasts cultured under differentiation conditions on control or VN-coated plates on day 1 and day 2 (n = 6), indicating enhanced proliferative activity under VN conditions. **d,** Representative immunofluorescence images showing myogenin and MHC expression in human LHCN-M2 myoblasts cultured under differentiation conditions on control or VN-coated substrates. Quantification of myogenin- and MHC-positive cells relative to total nuclei is shown (Control: n = 2,747; Vitronectin: n = 2,313 for myogenin; Control: n = 580; VN: n = 634 for MHC). **e,** Representative immunofluorescence images of MHC and DAPI staining in LHCN-M2 myoblasts. Fusion index is

View Article Online
DOI: 10.1039/D6BM00313C

quantified as the number of nuclei per MHC-positive myotube. For visualization 25% (b) and 50% (d) of data points were randomly sampled for dot plotting, while all data were used for statistical analysis. Scale bars: 100 µm (a, d), 50 µm (b, e). Nuclei were counterstained with DAPI. Data are presented as mean ± s.d. Statistical significance was determined using Student's t-test (**$p < 0.01$).

Figure 6 | Vitronectin suppresses differentiation and promotes proliferation in primary avian myoblasts

a, Experimental design of primary culture of embryonic chicken myoblasts. Fertilized eggs were incubated for 10 days, and myogenic cells were isolated from thigh muscle tissue. **b,** Representative immunofluorescence images for MHC. Differentiation was quantified by the number of nuclei per myotube. **c,** Relative cell numbers (n = 3). **d,** Representative immunofluorescence images for p-Histone H3. **e,** Representative spheroid images. Scale bars: 50 µm (a–c), 100 µm (d). Nuclei were counterstained with DAPI. Data are presented as mean ± s.d. Statistical significance was determined using Student's t-test (**$p < 0.01$).

References:

1 R. O. Hynes, *Science*, 2009, 326, 1216–1219.
2 C. Frantz, K. M. Stewart and V. M. Weaver, *Journal of Cell Science*, 2010, 123, 4195–4200.
3 F. G. Giancotti and E. Ruoslahti, *Science*, 1999, Vol 285, 1028–1033.

View Article Online
DOI: 10.1039/D6BM00313C

4 J. Ivaska and J. Heino, *Annu. Rev. Cell Dev. Biol.*, 2011, 27, 291–320.
5 H. Yin, F. Price and M. A. Rudnicki, *Physiological Reviews*, 2013, 93, 23–67.
6 C. F. Bentzinger, Y. X. Wang and M. A. Rudnicki, *Cold Spring Harbor Perspectives in Biology*, 2012, 4, a008342–a008342.
7 D. Yaffe and O. Saxel, *Nature*, 1977, 270, 725–727.
8 S. Burattini, P. Ferri, M. Battistelli, R. Curci, F. Luchetti and E. Falcieri, *European Journal of Histochemistry*, 2004, 48, 223–234.
9 C. H. Clegg, T. A. Linkhart, B. B. Olwin and S. D. Hauschka, *The Journal of cell biology*, 1987, 105, 949–956.
10 R. E. Allen and L. K. Boxhorn, *Journal of Cellular Physiology*, 1989, 138, 311–315.
11 A. Saini, E. Rullman, M. Lilja, M. Mandić, M. Melin, K. Olsson and T. Gustafsson, *PLoS ONE*, 2018, 13, e0192384.
12 R. Vaz, G. G. Martins, S. Thorsteinsdóttir and G. Rodrigues, *Cell Tissue Res*, 2012, 348, 569–578.
13 A. Ito, M. Yamamoto, K. Ikeda, M. Sato, Y. Kawabe and M. Kamihira, *Journal of Bioscience and Bioengineering*, 2015, 119, 596–603.
14 V. Chaturvedi, D. E. Dye, B. F. Kinnear, T. H. Van Kuppevelt, M. D. Grounds and D. R. Coombe, *PLoS ONE*, 2015, 10, e0127675.
15 M. Kim, H. Y. Jung, B. Kim and C. Jo, *Food Sci Anim Resour*, 2024, 44, 710–722.
16 E. S. Novoseletskaya, O. A. Grigorieva, A. Yu. Efimenko and N. I. Kalinina, *Biochemistry Moscow*, 2019, 84, 232–240.
17 P. Klaus T., *Annual Review of Cell and Developmental Biology*, 1991, Vol.7, 275–310.
18 E. G. Hayman, M. D. Pierschbacher, Y. Ohgren and E. Ruoslahti, *Proc. Natl. Acad. Sci. U.S.A.*, 1983, 80, 4003–4007.
19 B. P. Eliceiri, *Circulation Research*, 2001, 89, 1104–1110.
20 D. Yaffe, *Proc. Natl. Acad. Sci. U.S.A.*, 1968, 61, 477–483.
21 C. Zhu, V. Mouly, R. N. Cooper, K. Mamchaoui, A. Bigot, J. W. Shay, J. P. Di Santo, G. S. Butler-Browne and W. E. Wright, *Aging Cell*, 2007, 6, 515–523.
22 S. Takii, J. Wu and D. Okamura, *PLoS ONE*, 2022, 17, e0259482.
23 T. Katayama, M. Takechi, Y. Murata, Y. Chigi, S. Yamaguchi and D. Okamura, *Front. Bioeng. Biotechnol.*, 2024, 12, 1390386.
24 H. Niwa, K. Araki, S. Kimura, S. Taniguchi, S. Wakasugi and K. Yamamura, *The Journal of Biochemistry*, 1993, 113, 343–349.
25 T. Katayama, Y. Chigi and D. Okamura, *Front. Cell Dev. Biol.*, 2023, 11, 1193634.

View Article Online
DOI: 10.1039/D6BM00313C

26 Y.-N. Jang and E. J. Baik, *JAK-STAT*, 2013, 2, e23282.

27 K. Wang, C. Wang, F. Xiao, H. Wang and Z. Wu, *Journal of Biological Chemistry*, 2008, 283, 34029–34036.

28 M. K. Trenerry, P. Gatta and D. Cameron-Smith, *BMC Physiol*, 2011, 11, 6.

29 J. M. Maurice, Y. Gan, F. Ma, Y. Chang, M. Hibner and Y. Huang, *Acta Pharmacol Sin*, 2010, 31, 493–500.

30 D. D. Sarbassov, L. G. Jones and C. A. Peterson, *Molecular Endocrinology*, DOI:doi.org/10.1210/mend.11.13.0036.

31 A. Takahashi, Y. Kureishi, J. Yang, Z. Luo, K. Guo, D. Mukhopadhyay, Y. Ivashchenko, D. Branellec and K. Walsh, *Molecular and Cellular Biology*, 2002, 22, 4803–4814.

32 M. A. Dechantsreiter, E. Planker, B. Mathä, E. Lohof, G. Hölzemann, A. Jonczyk, S. L. Goodman and H. Kessler, *J. Med. Chem.*, 1999, 42, 3033–3040.

33 A. Mohan and A. Asakura, *JPFSM*, 2017, 6, 65–74.

34 V. Andrés and K. Walsh, *Journal of Cell Biology*, 1996, 132, 657–666.

35 I. Glauche, K. Moore, L. Thielecke, K. Horn, M. Loeffler and I. Roeder, *PLoS Comput Biol*, 2009, 5, e1000447.

36 A. E. Hochreiter-Hufford, C. S. Lee, J. M. Kinchen, J. D. Sokolowski, S. Arandjelovic, J. A. Call, A. L. Klibanov, Z. Yan, J. W. Mandell and K. S. Ravichandran, *Nature*, 2013, 497, 263–267.

37 P. Zhang, C. Wong, D. Liu, M. Finegold, J. W. Harper and S. J. Elledge, *Genes & Development*, 1999, 13, 213–224.

38 K. Guo, J. Wang, V. Andrés, R. C. Smith and K. Walsh, *Molecular and Cellular Biology*, 1995, 15, 3823–3829.

39 J. V. Chakkalakal, J. Christensen, W. Xiang, M. T. Tierney, F. S. Boscolo, A. Sacco and A. S. Brack, *Development*, 2014, 141, 1649–1659.

40 M. Yu, H. Wang, Y. Xu, D. Yu, D. Li, X. Liu and W. Du, *Cell Biology International*, 2015, 39, 910–922.

41 C. L. Sadowski, T. T. Wheeler, L.-H. Wang and H. B. Sadowski, *Endocrinology*, 2001, 142, 3890–900.

42 A. J. Kudla, N. C. Jones, R. Scott Rosenthal, K. Arthur, K. L. Clase and B. B. Olwin, *The Journal of Cell Biology*, 1998, 142, 241–250.

43 M. Mansouri and N. D. Leipzig, *Biophysics Reviews*, 2021, 2, 021305.

44 X. Wu, J. Su, J. Wei, N. Jiang and X. Ge, *Stem Cells International*, 2021, 2021, 1–13.

45 K. Stange, A. Keric, A. Friese and M. Röntgen, *Cells*, 2022, 11, 1453.

46 L. C. Hunt, A. Upadhyay, J. A. Jazayeri, E. M. Tudor and J. D. White, *Skeletal Muscle*, 2015, 5, 17.

47 C. Jo, H. Kim, I. Jo, I. Choi, S.-C. Jung, J. Kim, S. S. Kim and S. A. Jo, *Biochimica et Biophysica Acta (BBA) - Molecular Cell Research*, 2005, 1743, 187–197.

48 Z. Wu, P. J. Woodring, K. S. Bhakta, K. Tamura, F. Wen, J. R. Feramisco, M. Karin, J. Y. J. Wang and P. L. Puri, *Molecular and Cellular Biology*, 2000, 20, 3951–3964.

49 L. Sun, K. Ma, H. Wang, F. Xiao, Y. Gao, W. Zhang, K. Wang, X. Gao, N. Ip and Z. Wu, *Journal of Cell Biology*, 2007, 179, 129–138.

50 A. Cuenda and P. Cohen, *Journal of Biological Chemistry*, 1999, 274, 4341–4346.

51 K. R. Legate, S. A. Wickström and R. Fässler, *Genes Dev.*, 2009, 23, 397–418.

52 S. K. Mitra and D. D. Schlaepfer, *Current Opinion in Cell Biology*, 2006, 18, 516–523.

53 E. G. Kleinschmidt and D. D. Schlaepfer, *Current Opinion in Cell Biology*, 2017, 45, 24–30.

54 E. R. Horton, J. D. Humphries, B. Stutchbury, G. Jacquemet, C. Ballestrem, S. T. Barry and M. J. Humphries, *Journal of Cell Biology*, 2016, 212, 349–364.

55 X. Pang, X. He, Z. Qiu, H. Zhang, R. Xie, Z. Liu, Y. Gu, N. Zhao, Q. Xiang and Y. Cui, *Sig Transduct Target Ther*, 2023, 8, 1.

56 N. Alam, H. L. Goel, M. J. Zarif, J. E. Butterfield, H. M. Perkins, B. G. Sansoucy, T. K. Sawyer and L. R. Languino, *Journal Cellular Physiology*, 2007, 213, 649–653.

57 B. P. Eliceiri, *Circulation Research*, 2001, 89, 1104–1110.

58 E. Carraro, L. Rossi, E. Maghin, M. Canton and M. Piccoli, *Front. Bioeng. Biotechnol.*, 2022, 10, 941623.

59 L. Madden, M. Juhas, W. E. Kraus, G. A. Truskey and N. Bursac, *eLife*, 2015, 4, e04885.

60 S. M. Maffioletti, S. Sarcar, A. B. H. Henderson, I. Mannhardt, L. Pinton, L. A. Moyle, H. Steele-Stallard, O. Cappellari, K. E. Wells, G. Ferrari, J. S. Mitchell, G. E. Tyzack, V. N. Kotiadis, M. Khedr, M. Ragazzi, W. Wang, M. R. Duchen, R. Patani, P. S. Zammit, D. J. Wells, T. Eschenhagen and F. S. Tedesco, *Cell Reports*, 2018, 23, 899–908.

61 G. Chen, D. R. Gulbranson, Z. Hou, J. M. Bolin, V. Ruotti, M. D. Probasco, K. Smuga-Otto, S. E. Howden, N. R. Diol, N. E. Propson, R. Wagner, G. O. Lee, J. Antosiewicz-Bourget, J. M. C. Teng and J. A. Thomson, *Nat Methods*, 2011, 8, 424–429.

62 S. R. Braam, L. Zeinstra, S. Litjens, D. Ward-van Oostwaard, S. Van Den Brink, L. Van Laake, F. Lebrin, P. Kats, R. Hochstenbach, R. Passier, A. Sonnenberg and C. L. Mummery, *Stem Cells*, 2008, 26, 2257–2265.

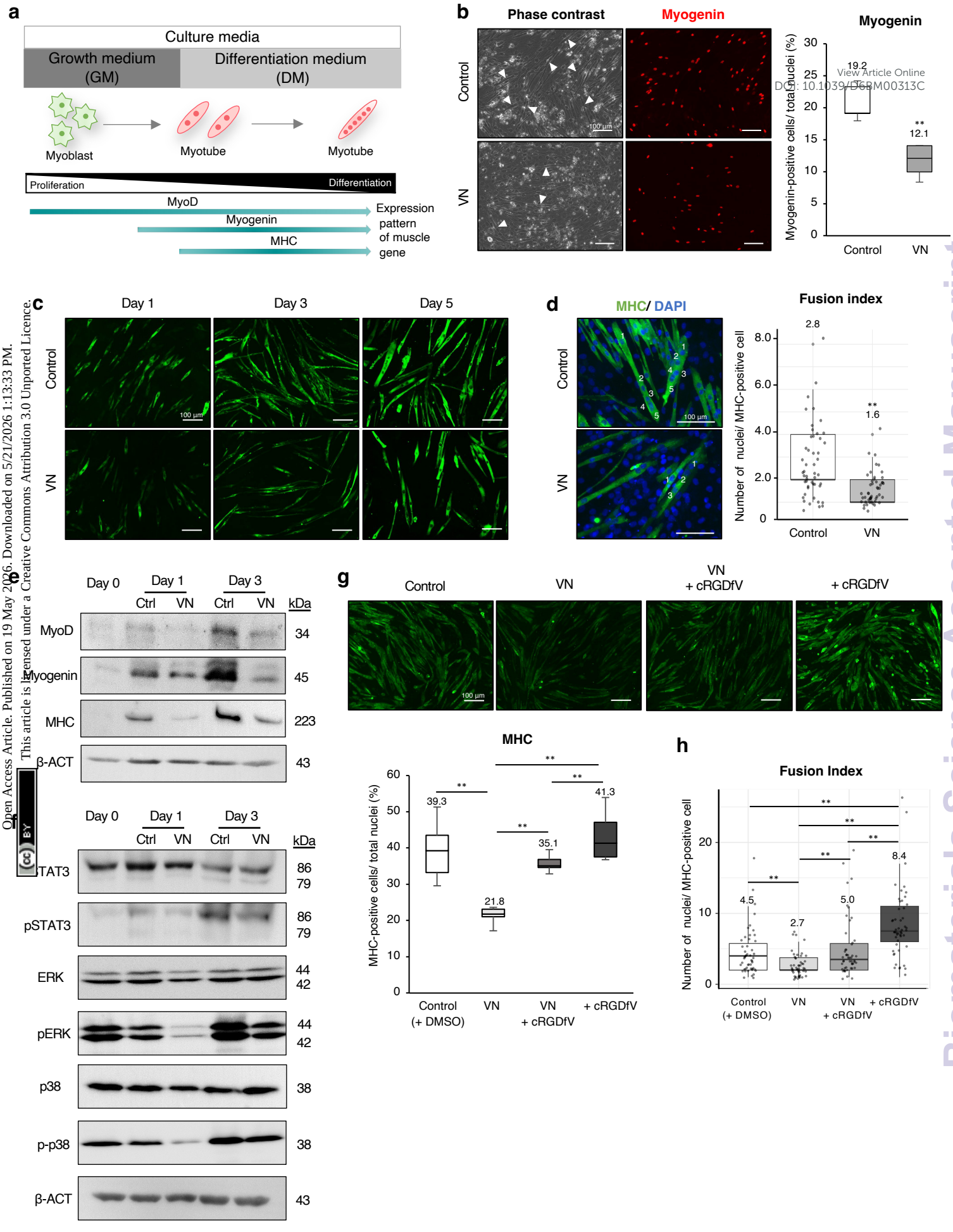

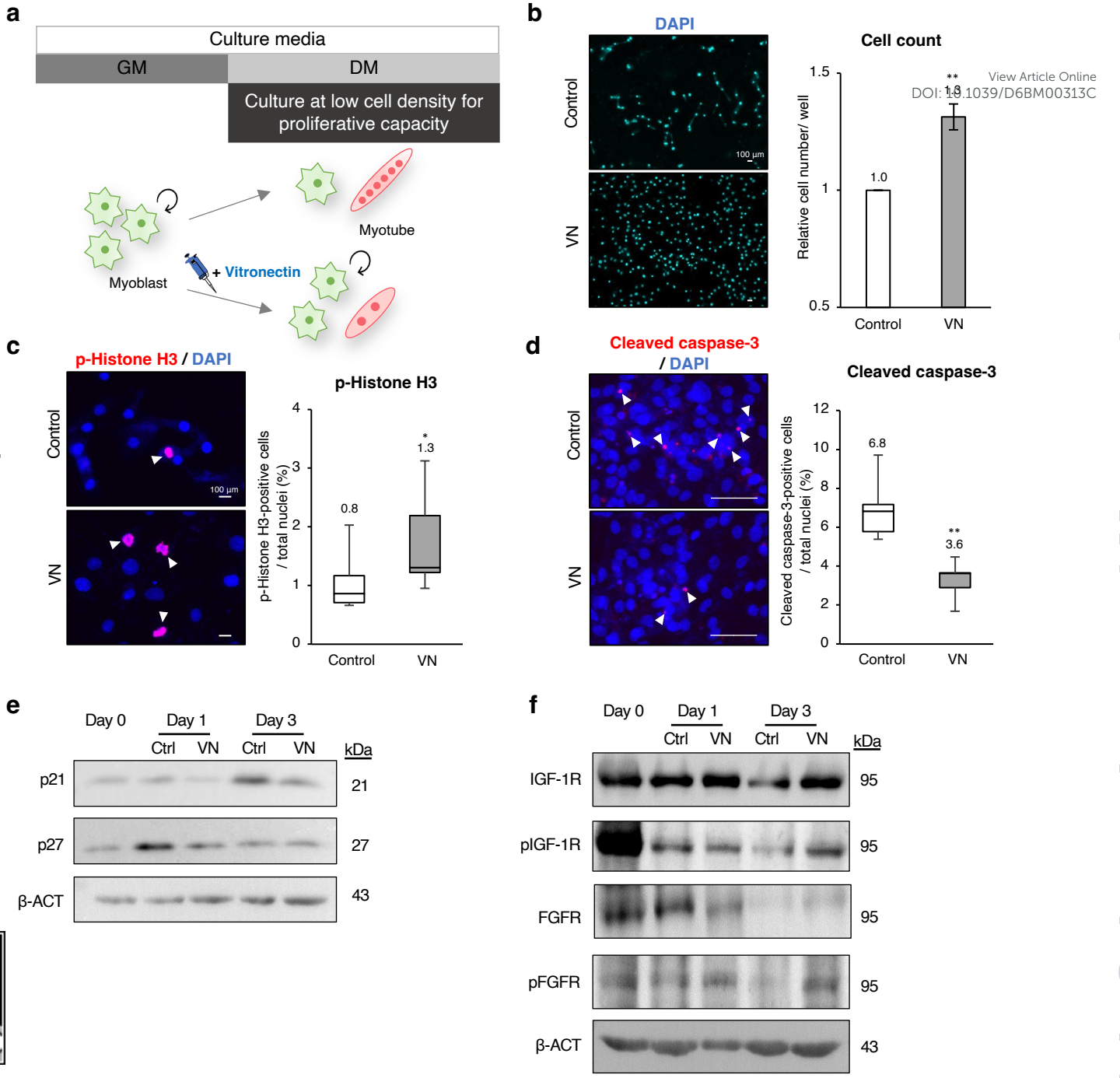

Figure 3

View Article Online
DOI: 10.1039/D6BM00313C

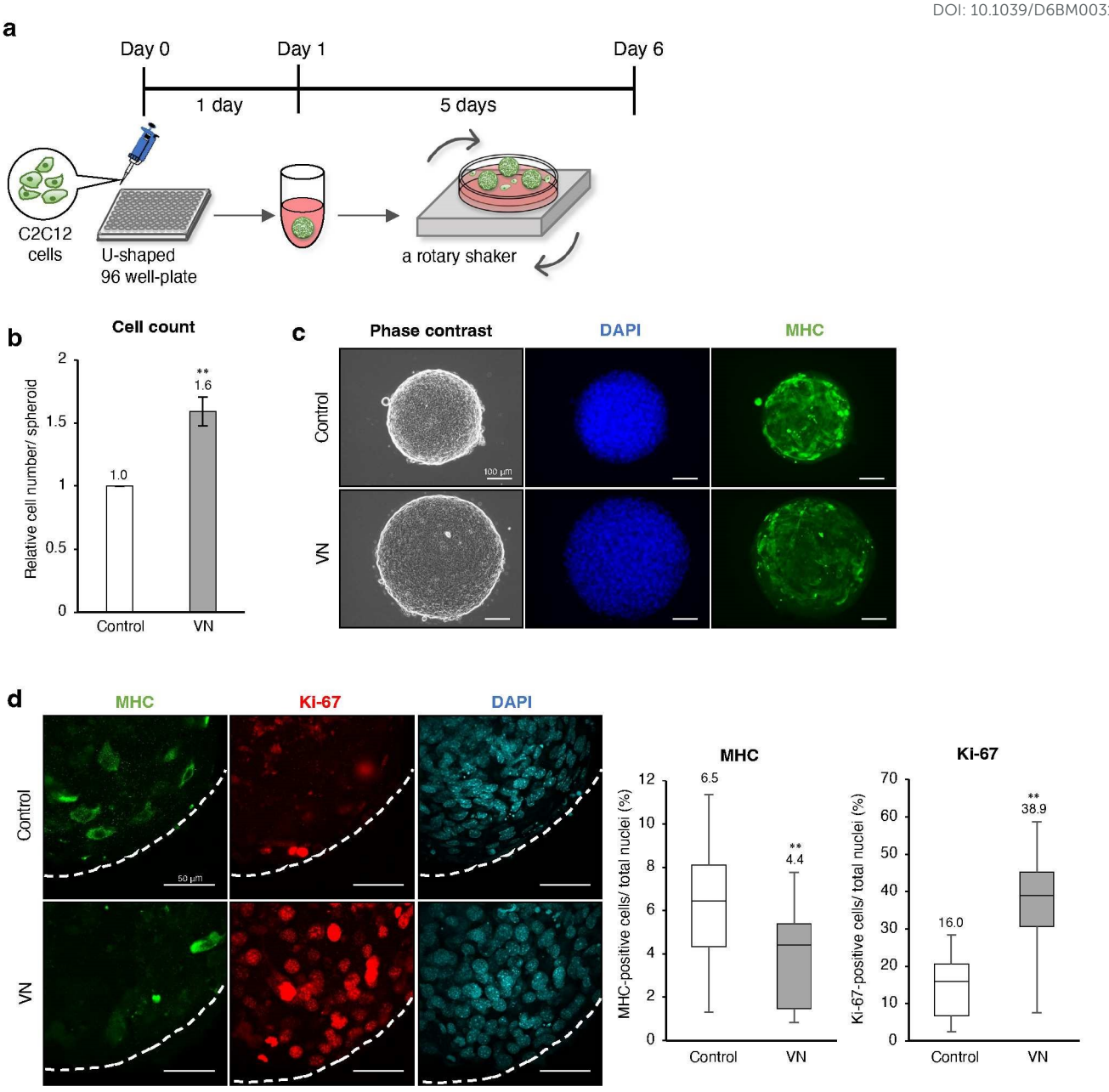

View Article Online
DOI: 10.1039/D6BM00313C

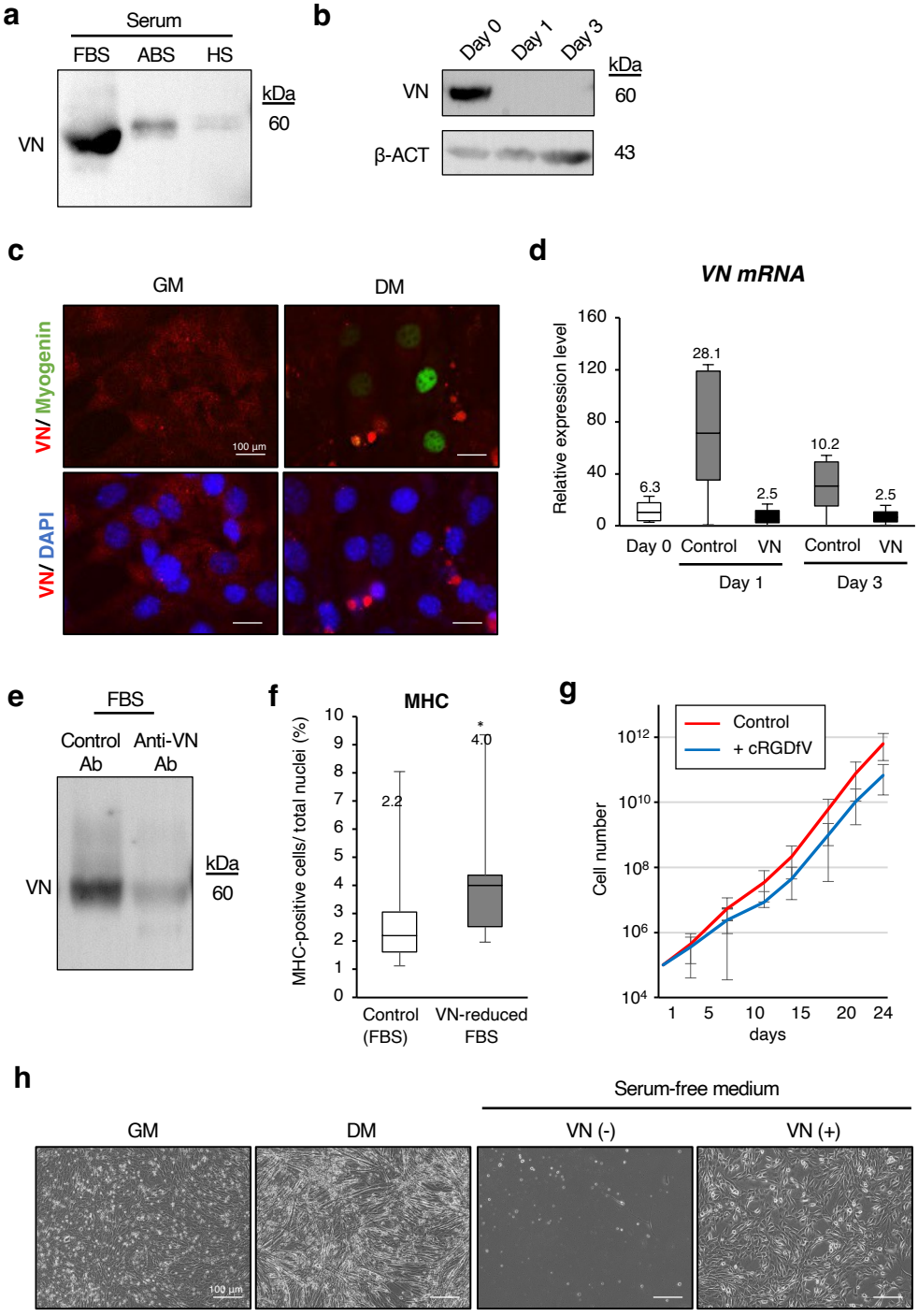

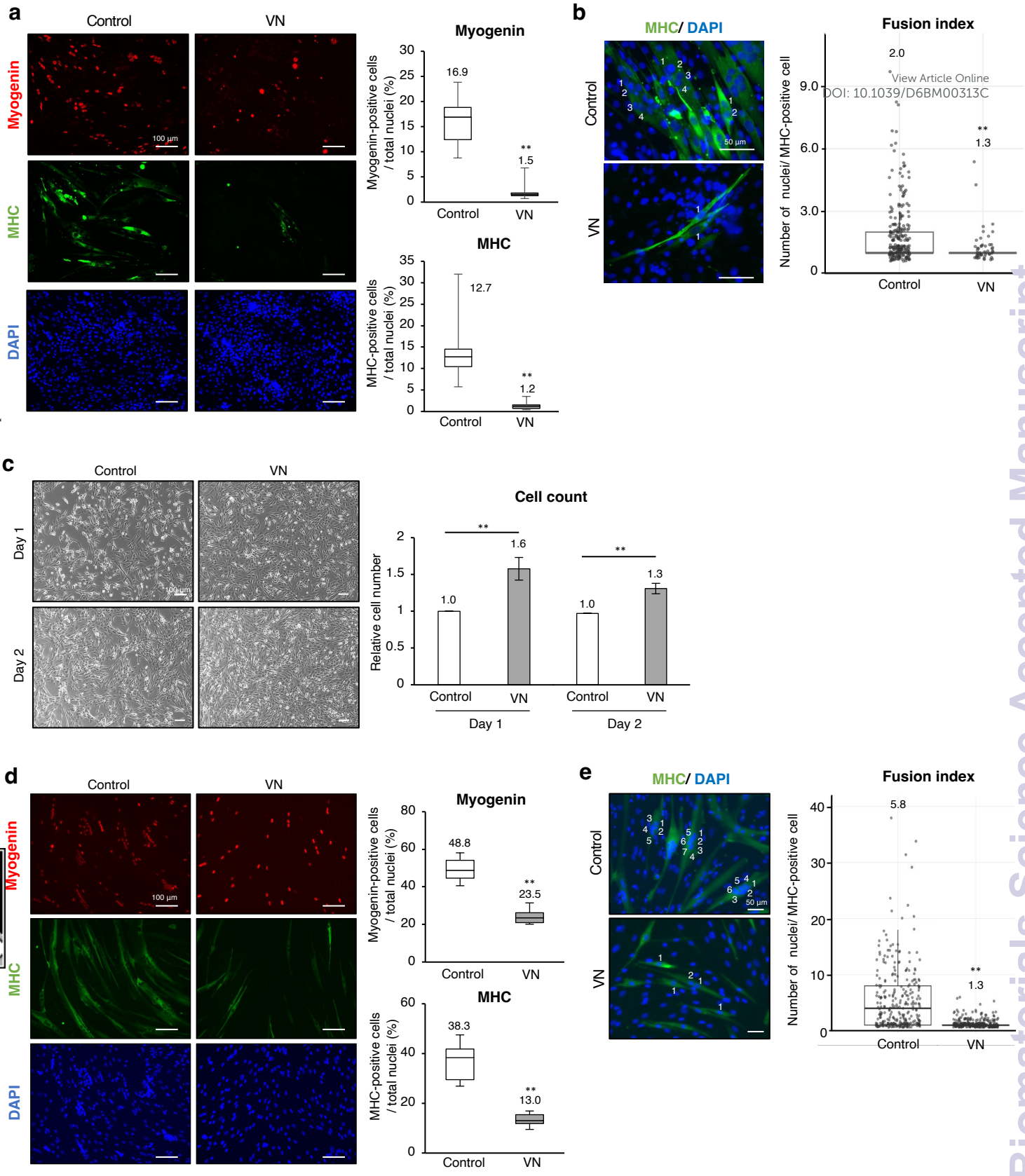

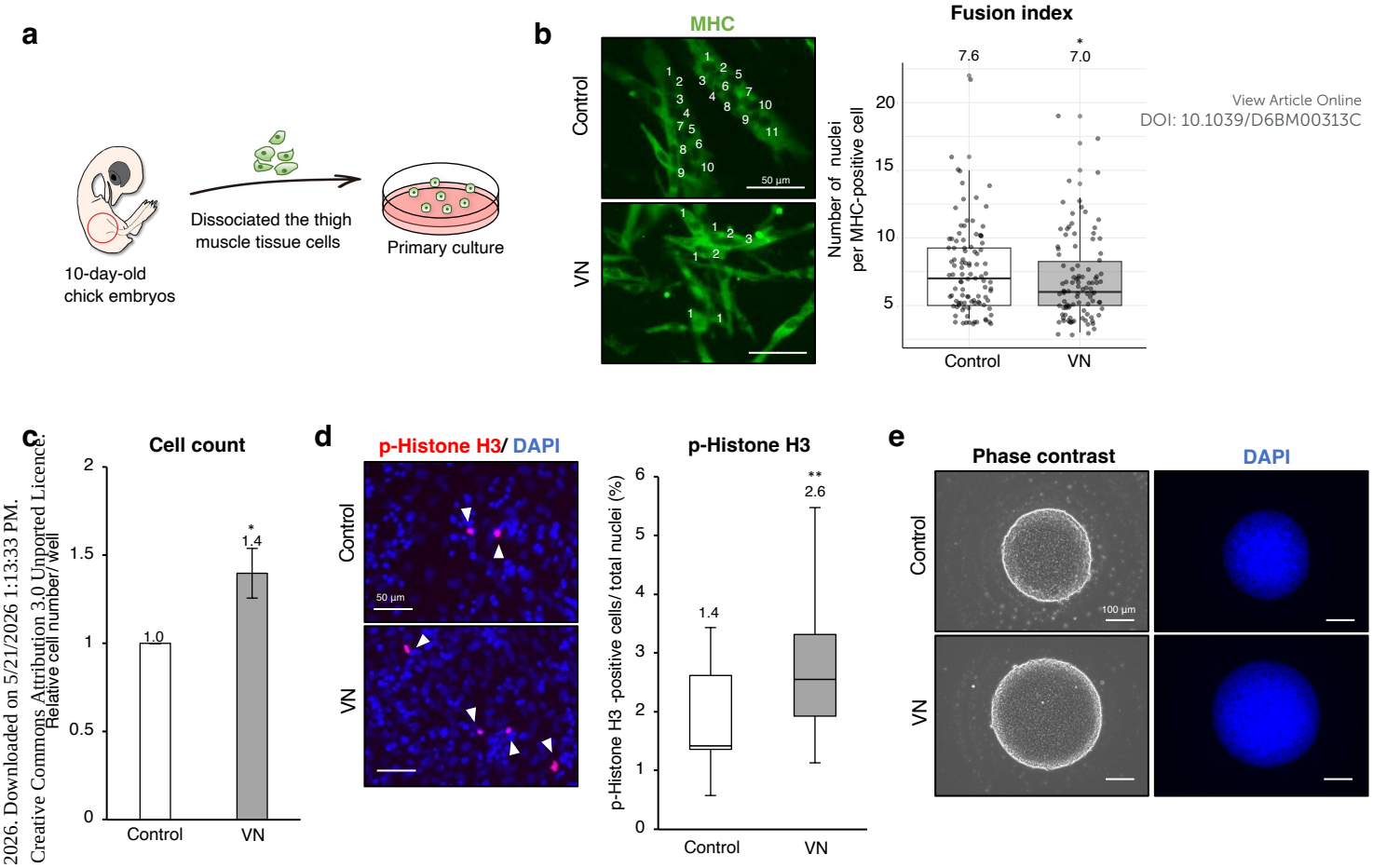

View Article Online
DOI: 10.1039/D6BM00313C

Data Availability Statement

The data supporting the findings of this study are available within the article and its Supplementary Information. This includes quantitative datasets underlying the graphs, uncropped immunoblot images, and additional experimental details necessary to reproduce the reported results.